

Fire-spotting modelling in operational wildfire simulators based on Cellular Automata: A comparison study

Marcos López-De-Castro ^{a,1}, Andrea Trucchia ^b, Umberto Morra di Cella ^b, Paolo Fiorucci ^b, Antonio Cardillo ^c, Gianni Pagnini ^{a,d,*}

^a BCAM – Basque Center for Applied Mathematics, Alameda de Mazarredo 14, Bilbao, 48009, Basque Country, Spain

^b CIMA Research Foundation, Via Armando Magliotto 2, 17100, Savona, Italy

^c Regione Molise, Centro Funzionale Decentrato del Molise, Contrada Selva del Campo, Campochiaro, 86020, Italy

^d Ikerbasque – Basque Foundation for Science, Plaza Euskadi 5, Bilbao, 48009, Basque Country, Spain

ARTICLE INFO

Dataset link: <https://gitlab.bcamath.org/malopez/fire-spotting.git>

Keywords:

Fire-spotting
Spot-fires
Fire spread
RandomFront
Wildfires
Cellular Automata

ABSTRACT

One crucial mechanism in the spread of wildfires is the so-called fire-spotting: a random phenomenon that occurs when embers are transported over large distances. Fire-spotting speeds up the rate of spread and starts new ignitions that can jeopardise firefighting operations. Unfortunately, operational fire-spread simulators may not account for spotting events, thus overlooking the harmful consequences associated with this phenomenon. In this work, three fire spotting parametrisations are integrated in the operational wildfire simulator PROPAGATOR based on Cellular Automata (CA). RandomFront, a physics-based parametrisation of fire-spotting, is tested for the first time in the context of CA simulators. RandomFront is compared with other two parametrisations already adopted in CA based simulators, those by Alexandridis and co-authors and by Perryman and collaborators. A wildfire occurred in the summer of 2021 in the municipality of Campomarino (Molise, Italy), and where spotting effects were clearly reported, is used as a case study. This case study, featuring evident airborne transport of firebrands, paves the way for a framework for comparing parameterised spotting models used in operational scenarios. RandomFront produced a more complex burning probability pattern than the other parametrisations and it predicted a higher probability of burning in the zone mainly affected by the fire-spotting.

1. Introduction

Accurate predictions of wildfire behaviour are essential for improving fire risk assessment (Calkin et al., 2011), aiding fire management decision-making and mitigating wildfire impacts (Stephenson et al., 2013). Unfortunately, wildfire propagation is a complex phenomenon that involves multiple physical and chemical processes, leading to numerous sources of uncertainty (Benali et al., 2016). One of these sources of uncertainty is the so called *fire-spotting phenomenon*. Fire-spotting is strongly influenced by atmospheric conditions and vegetation types and occurs when firebrands are carried away from the original fire and ignite secondary fires, known as spot-fires (Brown and Davis, 1973; Bhutia et al., 2010; Werth et al., 2011). Those new fires can occur near the fire propagation front, being able to increase the Rate of Spread (ROS) (Storey et al., 2021), or several kilometres away from the primary fire, leading to new secondary ignitions. This increases the

risk for both civilians and firefighters, who may become trapped by secondary fronts ignited by firebrands (Koo et al., 2010; Storey et al., 2020).

The research conducted for understanding and reproducing fire-spotting falls into two main approaches. On one hand, experimental studies have focused on characterising firebrands (weight, size, generation mechanism ...) and its transport process (Manzello et al., 2007, 2008; Suzuki et al., 2012; Thomas et al., 2017; Storey et al., 2021; Himoto and Iwami, 2021). However, the small scales of the experiments limit their direct application in estimating landing distribution during real-world wildfires (Pérez et al., 2011; Sullivan and Cruz, 2015; Egorova et al., 2022). On the other hand, firebrand transport mathematical models have been developed to estimate the landing distribution and flight paths of firebrands (Wadhvani et al., 2022a). An early firebrand transport model was proposed by Tarifa et al. (1965,

* Corresponding author at: BCAM – Basque Center for Applied Mathematics, Alameda de Mazarredo 14, Bilbao, 48009, Basque Country, Spain.

E-mail address: gpagnini@bcamath.org (G. Pagnini).

¹ Present affiliations: DATAI - Institute of Data Science and Artificial Intelligence, Universidad de Navarra, Edificio Ismael Sánchez Bella, Campus Universitario, 31009, Pamplona, Navarre, Spain. TECNUN School of Engineering, Universidad de Navarra, Donostia-San Sebastián, Basque Country, Spain.

1967), who studied travel distances based on firebrand size, density, and shape, and by [Albini \(1979, 1983\)](#), who estimated the maximum distance of new ignitions in terms of the burning area and mean wind. These models are integrated into wildfire spread simulation models such as FARSITE ([Finney, 1998](#)), Phoenix Rapidfire ([Tolhurst et al., 2008](#)) or Prometheus ([Tymstra et al., 2010](#)). [Himoto and Tanaka \(2005\)](#) proposed a transport model for disk-shaped firebrands. They suggested that the lognormal distribution is suitable for describing the landing distribution of firebrands in the downwind direction, while the normal distribution is appropriate for the perpendicular direction. [Sardoy et al. \(2007, 2008\)](#) conducted numerical experiments that incorporated atmospheric conditions, fire and fuel properties. As [Himoto and Tanaka \(2005\)](#) and [Sardoy et al. \(2007, 2008\)](#) found that the distribution of firebrand landing distances follows a log-normal distribution. [Wang \(2011\)](#) developed a mathematical model that derives the firebrand distribution and mass from a Rayleigh distribution function.

The physical parametrisation of fire-spotting is a crucial aspect to consider for obtaining reliable predictions ([Fernandez-Pello, 2017](#)). Unfortunately, conducting fire-spotting simulations using computational fluid dynamic codes ([Richards, 2010](#); [Wadhvani et al., 2017](#); [Tohidi and Kaye, 2017](#); [Wadhvani et al., 2022b](#)) involves the challenging task of resolving the equations that govern mass, momentum, and energy transport. This process often exceeds the time frame typically suitable for the decision-making process in wildfire management. The fire-spotting parametrisation *RandomFront* was developed to overcome this issue ([Pagnini and Mentrelli, 2014](#); [Kaur et al., 2016](#); [Trucchia et al., 2019](#)). This parametrisation is independent of the formulation of the ROS and of the method utilised for the fire-line advancement, such as the Level Set Method used in LSFire+ ([Pagnini and Mentrelli, 2014](#)), WRF-Sfire, [Trucchia et al. \(2019\)](#), and the Lagrangian Discrete Event System Specification (DEVs) adopted by ForeFire ([Kaur et al., 2016](#)). *RandomFront* has been successfully implemented in the semi-physical model PhyFire, which is based on principles of energy and mass conservation ([Asensio et al., 2021](#)). Moreover, *RandomFront* includes the effects of atmospheric stability by considering the height of the Atmospheric Boundary Layer, as well as the effects of terrain slope and flame geometry ([Egorova et al., 2020, 2022](#)).

Here, the *RandomFront* parametrisation is implemented for the first time within the operational wildfire spread simulator *PROPAGATOR* that is based on a Cellular Automata (CA) approach ([Trucchia et al., 2020](#)). Two other parametrisations are also implemented in the simulator, namely those introduced by [Alexandridis et al. \(2008, 2011\)](#) and by [Perryman et al. \(2013\)](#). The parametrisations of [Alexandridis et al.](#) and [Perryman et al.](#) and *RandomFront* are characterised by an increasing complexity while still maintaining operational feasibility. The effects of changing parametrisation in a set of synthetic test cases, with uniform wind, fuel, and topography, are analysed, in order to depict the characteristic fire spotting patterns related to each formulation.

Finally, the fire spread simulator *PROPAGATOR* is used to simulate a wildfire which took place in 2021 in the municipality of Campomarino (Molise, Italy), testing each one of the aforementioned fire-spotting routines. The final burnt area comprised two main fire perimeters separated by a water body, and fire spotting was reported during the response phase. Thus, this real case study represents a good benchmark for assessing the performance of a CA-based fire spread simulator featuring a fire spotting module, and also for comparing the performance among different fire spotting parametrisations.

The paper is organised as follows: in Section 2 a general description of the fire-spread model and of the fire-spotting parametrisations is provided. In Section 3 the methodology of the study is described, and in Section 4 the results of the simulations are reported. Section 5 contains the discussion of the results while in Section 6 conclusions are presented.

2. Models description

In this section, first we introduce the operational fire-spread model *PROPAGATOR*, which is based on a CA approach. Three different fire-spotting parametrisations are then presented.

2.1. Mathematical modelling and wildfires

Several approaches have been developed to model and simulate wildfire behaviour ([Sullivan, 2009a,b,c](#)). Simulators based on CA approach offer successful advantages in operational use due to their flexibility and a reduced computational cost. Formally, a two-dimensional cellular automaton is defined as an ultra-discrete dynamical system given by the 4-tuple $\mathcal{A} = (\mathcal{E}, \mathcal{S}, \mathcal{V}, f)$, where \mathcal{E} is the computational domain where the cells are defined, known as cellular space, the set of states \mathcal{S} represents the finite, or infinite, set of possible states in which each cell can be found at any given time step, \mathcal{V} represents the set of neighbouring cells surrounding a specific cell, whose states can influence the transition of the considered cell to a different state, and f denotes the transition rule between states.

In wildfire research, the computational domain \mathcal{E} is usually discretised into square cells ([Clarke et al., 1994](#)), although hexagonal cells have also been used ([Trunfio, 2004](#); [Encinas et al., 2007](#)). The rules governing the spreading of the fire from one cell to another, i.e., f , primarily depend on the states of neighbouring cells, i.e., \mathcal{V} , and they take into account also many factors such as vegetation type, wind field, terrain slope, as well as other physical parameters that contribute to the ROS ([Duarte, 1997](#); [Hargrove et al., 2000](#)). In this study, we use the fire-simulator *PROPAGATOR* for simulating the spread of the fire. The performance of *PROPAGATOR* in reproducing the behaviour of a number of wildfires that occurred in Mediterranean countries has been already discussed in a previous work by [Trucchia et al. \(2020\)](#). However, fire-spotting was not included at that stage. *PROPAGATOR* is an operational software developed for the Italian Civil Protection, based on a bi-dimensional cellular automaton approach. It incorporates high-resolution data on topography and land fuel cover. The fire-spread is computed using a probabilistic approach that takes into account several factors, including the vegetation type, terrain slope, wind direction and speed, and fine fuel moisture content. Given an ignited cell, wildfire can potentially spread through its Moore neighbourhood of range one (i.e., to its eight surrounding cells), at each time step. The resulting burnt area evolves randomly by providing static maps that account for elevation and fuel type. User input parameters for the simulation are the synoptic evolution of wind speed, wind direction, and fine fuel moisture content, as well as the ignition point. *PROPAGATOR* is specifically designed to generate at each time step a georeferenced map that indicates the probability of each cell of being burnt. This burning probability map follows a frequentist interpretation of probability, i.e., an ensemble of N independent simulations is performed and the burning probability assigned to the cell i at each time-step t is calculated by

$$p_i^t = \sum_{\omega=1}^N \frac{n_i^{t,\omega}}{N}, \quad (1)$$

where ω labels each independent realisation with $1 \leq \omega \leq N$ and

$$n_i^{t,\omega} = \begin{cases} 1 & : \text{ burnt cell,} \\ 0 & : \text{ unburnt cell.} \end{cases} \quad (2)$$

2.2. Fire-spotting models

Despite the demonstrated ability of CA-based models to replicate wildfire behaviour, fire-spotting remains not considered or, when it is included, it is based on pure probabilistic assumptions that disregard relevant physical features. In this subsection, we present three fire-spotting models for their comparison. The three models are presented in order of increasing complexity. The last two formulations

(Perryman and RandomFront) include also buoyancy and employ a lognormal probability density function for the spotting distance. The first two formulations were originally proposed for a CA framework, while RandomFront is implemented in a CA scheme for the first time.

2.2.1. The Alexandridis et al. fire-spotting parametrisation

The fire-spotting model formulated by Alexandridis et al. (2008, 2011) was designed specifically for a CA framework where the vegetation type and density, wind field and topography are the input layers. In the original model, the spotting phenomenon is just another trigger for the cell status transition. In their original works, simulations were focused on fires occurred in Greece, in the Spetses island and in the Attica region, showing a satisfactory performance. Freire and DaCamara (2019) slightly refactored the model to simulate a wildfire that occurred in Algarve region, Portugal.

The model computes the firebrand landing distance d as follows:

$$d = r_n \cdot P_w = r_n \exp(U \cdot C_v (\cos(\varphi) - 1)), \quad (3)$$

where r_n is a random number drawn from a normal distribution, φ is the angle between the wind direction and the direction of the ejected firebrand and it is drawn from a uniform distribution, U is the mean-wind velocity, and C_v is a vegetation-dependent fitted constant. A second part concerns the spot ignition, i.e., if an ejected firebrand will ignite or not a new spot-fire. This probability is computed by:

$$P_c = \begin{cases} P_{c0} (1 + P_{cd}), & \text{if } P_{c0} (1 + P_{cd}) \leq 1, \\ 1, & \text{if } P_{c0} (1 + P_{cd}) > 1, \end{cases} \quad (4)$$

where P_{c0} is a constant probability corrected by P_{cd} which depends on type and density of the fuel. This model is similar to the SPOT module implemented in BEHAVE (Andrews, 1986, 2014).

2.2.2. The Perryman et al. fire-spotting parametrisation

Perryman et al. (2013) developed a CA-based system and studied how spotting affects the ROS in a *Pinus ponderosa* ecosystem. The model consists in a suite of four sub-models adapted to a cellular automaton environment. These sub-models are used to compute the surface spread, tree torching probability, firebrand landing distribution and the spot ignition. The firebrand landing distance is calculated as the Euclidean distance between the firebrand landing distance parallel to the wind and the firebrand landing distance perpendicular to the wind. The distribution of firebrands in the direction parallel to the wind is implemented by following the statistical findings of Sardoy et al. (2008), where the landing distance follows a lognormal distribution function:

$$P(d) = \frac{1}{\sqrt{2\pi} \sigma d} \exp \left\{ -\frac{(\ln(d/\mu))^2}{2\sigma^2} \right\}, \quad (5)$$

where d is again the firebrand landing distance. Parameters μ and σ are established according to buoyancy driven or wind driven regimes. To distinguish between both cases, the Froude number Fr needs to be introduced. It is defined as:

$$Fr = \frac{U}{\sqrt{g \left(\frac{I_f}{\rho c_p T_A g^{1/2}} \right)^{2/3}}}, \quad (6)$$

where g is the acceleration of the gravity, I_f is fire intensity, ρ is the ambient gas density, c_p is the specific heat of gas, T_A is the ambient temperature and U is the wind speed. For a Froude number less than or equal to 1, a buoyancy-driven regime occurs, and we have:

$$\begin{cases} \sigma = 0.86 \left(\left(\frac{I_f}{I_{f0}} \right)^{-0.21} \left(\frac{U}{U_0} \right)^{0.44} \right) + 0.19, \\ \mu^* = 1.47 \left(\left(\frac{I_f}{I_{f0}} \right)^{0.54} \left(\frac{U}{U_0} \right)^{-0.55} \right) + 1.14, \end{cases} \quad (7)$$

and for Froude number greater than 1, wind driven regime occurs and we have:

$$\begin{cases} \sigma = 4.95 \left(\left(\frac{I_f}{I_{f0}} \right)^{-0.01} \left(\frac{U}{U_0} \right)^{0.02} \right) - 3.48, \\ \mu^* = 1.32 \left(\left(\frac{I_f}{I_{f0}} \right)^{0.26} \left(\frac{U}{U_0} \right)^{0.11} \right) + 0.02, \end{cases} \quad (8)$$

where $\mu = d_0 e^{\mu^*}$, d_0 , I_{f0} and U_0 have units of length ([m]), fireline intensity ([MW/m]), and speed ([m/s]), respectively. The assumption of Himoto and Tanaka (2005) is followed for firebrands travelling perpendicular to the mean-wind direction, i.e., the firebrand landing distance is modelled by means of a normal distribution, assuming a zero mean and standard deviation equal to the half of the automata's cell-size.

2.2.3. The RandomFront fire-spotting parametrisation

RandomFront parametrisation models the landing distance d by means of a log-normal distribution, see Eq. (5), combined with the physics involved in the transport of the firebrands (Trucchia et al., 2019).

The parameter μ of the log-normal distribution takes into account the essential factors needed to describe the lifting mechanism inside the convective column of the firebrands, and depends on the Atmospheric Boundary Layer (Egorova et al., 2020):

$$\mu = H \left(\frac{3 \rho C_d}{2 \rho_f} \right)^{1/2}, \quad (9)$$

where C_d is the Drag coefficient, ρ is the ambient gas density and ρ_f is the density of the wildland fuels. The maximum loftable height H is computed as a fraction of the injection height $H = 0.4 \cdot H_{smoke}$. The injection height of the smoke H_{smoke} follows the formula developed by Sofiev et al. (2012):

$$H = 0.4 \cdot H_{smoke} = 0.4 \left[\alpha H_{ABL} + \beta \left(\frac{I_f}{d P_{f0}} \right)^\zeta \exp \left(-\frac{\delta_{FT} N_{FT}^2}{N_0^2} \right) \right], \quad (10)$$

where H_{ABL} is the height of the Atmospheric Boundary Layer, N_{FT}^2 and N_0^2 are the Brunt-Väisälä frequency at the current height and in the free troposphere respectively, I_f is the fireline intensity and P_{f0} is the ratio of reference fire power.

The parameter σ of the log-normal distribution involves the effects of the horizontal wind in the transport of the firebrands and the effects of the flame geometry and the terrain slope in the spot pattern. The flame length is defined as Egorova et al. (2022):

$$L_f = \left(\frac{1}{2g(c_p T_A)^2} \right)^{1/3} I_f^{2/3}, \quad (11)$$

and if we denote by ψ the angle of the slope, φ the angle between the wind direction and the direction of the ejected firebrand and define $c_1(\psi) = \sqrt{g r (1 + \tan^2 \psi)}$, $c_2 = \beta_2 \sqrt{\frac{2\rho_f}{3\rho C_d}}$ and $c_3 = \sqrt{g L_f}$, then σ results to be (Egorova et al., 2022)

$$\sigma = \frac{1}{z_p} \ln \left(\frac{U \cos \varphi}{c_1(\psi)} + c_2 \frac{1.4U \cos \varphi + c_3 \tan \psi}{c_3 - 1.4U \cos \varphi \tan \psi} \right). \quad (12)$$

In the RandomFront parametrisation fire-spotting is a downwind phenomenon. Following this idea, a critical angle ϕ_0 is defined when $\sigma = 0$ such that no firebrands are emitted when $\sigma \leq 0$.

3. Materials and methods

Before performing simulations, two additional processes must be characterised for the complete integration of fire spotting modules into PROPAGATOR: firebrand generation and secondary ignitions (Storey et al., 2020; Liu et al., 2021). Despite research experiments at laboratory scale, see Manzello et al. (2020) and Liu et al. (2021), there is

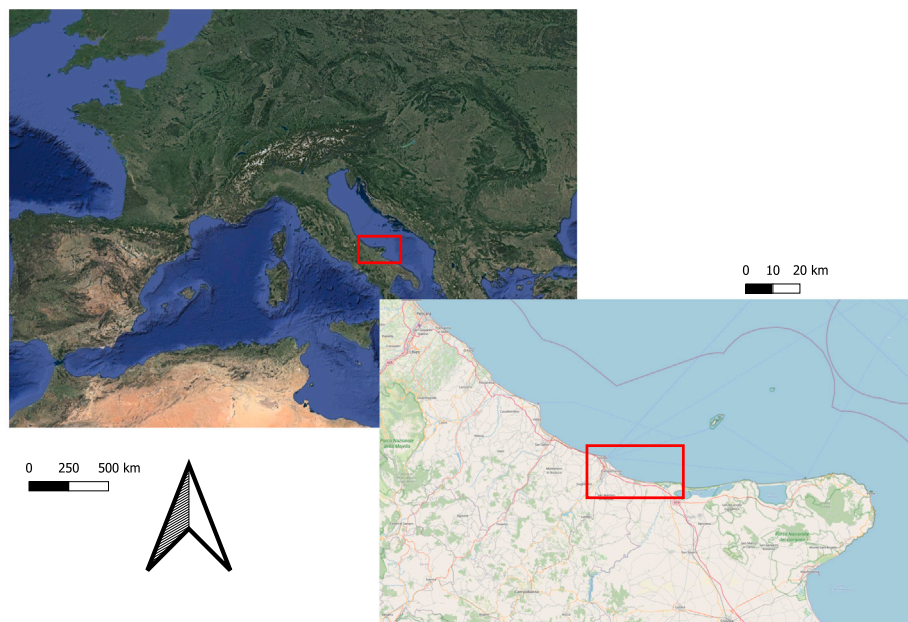


Fig. 1. Location of the studied area, in the Italian region of Molise, close to the municipality of Campomarino. Both pictures were obtained from the Google Earth and Google maps plugin in QGIS.

a lack of statistical studies describing suitable probability distributions for both phenomena. Therefore, for simplicity, we adopt the modelling choices described in Alexandridis et al. (2008). We assume that the number of firebrands ejected at each time-step follows a Poisson distribution, where the emission of one firebrand does not affect subsequent emissions. The Poisson distribution is well-suited to generate integer values of events that take place in a given time period. The probability of spot ignition, instead, is computed using Eq. (4).

The comparison study of the presented fire spotting algorithms is divided in two steps. For a preliminary analysis, wildfire simulations are performed under a synthetic setting with ideal conditions. This allows us to study how the spread patterns may change under different wind conditions for each fire spotting formulation. After that, the case study of Campomarino fire, described in Section 3.2, is simulated with PROPAGATOR fed by realistic wind and fuel conditions, without fire spotting module and with the three analysed fire spotting parametrisations. This particular wildfire presents a unique scenario. Firebrands flew over a water body to ignite a secondary fire, with eyewitness accounts detailing the timing of spotting occurrences. In this section we describe the experimental settings and the evaluation methods.

3.1. The synthetic test case

We define a quadrangular study area of 40 km² such that long-range spotting effects can be observed. Uniform vegetation cover is assumed, as well as a uniform fine fuel moisture content (set to 5%). In particular, the vegetation cover chosen is the PROPAGATOR calibrated class *Fire-Prone Conifers*, see Trucchia et al. (2020) for further information. Plain terrain, as well as constant speed and direction of the wind, are assumed during the simulations. The comparison study is performed under different constant wind speeds from South, without perturbations. In particular, we follow the Beaufort scale, where wind speed of 2.77 m s⁻¹ (10 km h⁻¹) is considered as *weak* and starting from 11.11 m s⁻¹ (40 km h⁻¹) is considered as *strong*.

The rest of the parameters used in the simulations are reported in Table 1. To avoid the use of arbitrary parameters in this set of experiments, any other parameter is kept consistent with the setting described in Section 3.2.

3.2. The case study of Campomarino fire

The wildfire occurred in a fire-prone conifers forest situated in the municipality of Campomarino, Molise region, along the Adriatic coast of Italy, see Fig. 1, on August 1st, 2021. The fire was ignited around 12:00 p.m. and was extinguished at 5:00 p.m. The studied area is depicted before and after the wildfire occurrence in Fig. 2. A tourist port, with a width of approximately 190 m, acted as a barrier to the spread of fire. This water body effectively divides the computational domain into two separate areas and prevents the transmission of fire by surface spread, highlighting thus the role of spotting effects. For simplicity, we will refer to both areas in this paper as the *West part of the port* or *secondary domain* and *East part of the port* or *main domain*. Firefighting efforts were reported in the South-East and in the North-West parts of the fire perimeter. Squads of volunteers of the regional Civil Protection reported instances of fire-spotting from the East side of the port to the West side approximately 3 h after the fire start.

To perform the simulations, we define a computational domain covering 2.98 km². The side of each cellular automaton cell corresponds to a longitude of 20 m. For each fire-spotting parametrisation, a PROPAGATOR run generates an ensemble of 100 independent realisations to calculate the burning probabilities. The number of realisations performed is obtained from the previous research (Trucchia et al., 2020). The fuel types used are adapted from the CORINE land cover classification (Feranec et al., 2016) to calibrated classes in PROPAGATOR (See Fig. 3). The main burnt area predominantly consists of a coniferous forest fuel type. Therefore, for the purposes of our study, we focus on fire-spotting phenomena resulting specifically from the fire-prone coniferous fuel type. In the studied area, the coniferous tree species associated with this fuel type are *Pinus Pinaster Aiton*. The data labelled as “non-burnable” have a low but non-zero probability of being burnt. The orography data are derived from a 20-meter Digital Elevation Model (DEM) provided by Italian Institute for Environmental Protection and Research (ISPRA).

The weather conditions during the wildfire were reported as unstable and turbulent, with speed peaks up to 19.44 m s⁻¹ (70 km h⁻¹). To reproduce these conditions, we consider a constant wind speed of 11.11 m s⁻¹ (40 km h⁻¹) and at every 9×10^2 s (15 min) interval of simulated time a random perturbation is added to the constant wind speed. The perturbation is derived by sampling a random variable from

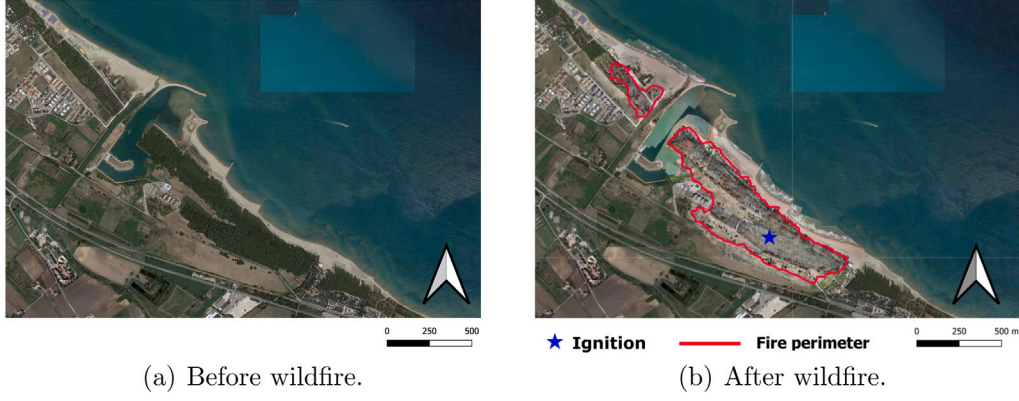


Fig. 2. Satellite imagery of the studied area. Figure (a) shows the area before the wildfire occurrence and was obtained from Google Earth through Qgis. Figure (b) shows the true colour orthomosaic derived by the UAV (unmanned aerial vehicle) survey conducted after the wildfire occurrence. The red line defines the burnt area, based on high resolution photo-interpretation. The blue dot indicates the approximate point where the fire started. The wildfire lasted approximately 5 h.

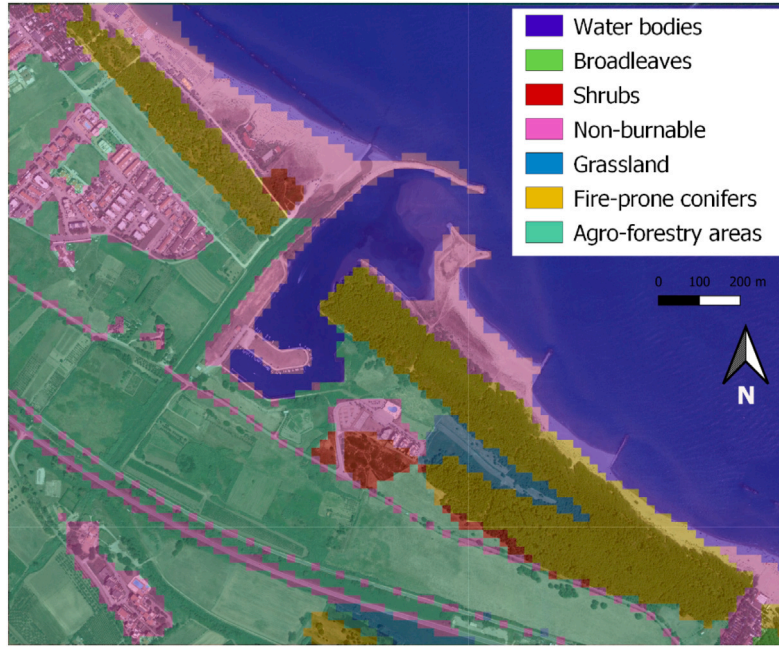


Fig. 3. Fuel type distribution over the simulated area. The data were obtained from the CORINE land cover classification and adapted to the PROPAGATOR fuel classification. The resolution for each cell is $20 \text{ m} \times 20 \text{ m}$. Areas classified as “Non-burnable” stand for areas with very low probability of fire spreading (such as built-up areas), but where fire spotting effects can still have an impact on infrastructure and exposed elements.

a normal distribution with zero mean and standard deviation of 5.55 m s^{-1} (20 km h^{-1}). Furthermore, we account for variations in the main wind direction, which was predominantly reported as flowing from South to North. The perturbations to the main wind direction are also introduced every $9 \times 10^2 \text{ s}$ (15 min), using another random variable obtained from a normal distribution with zero mean and standard deviation of 22.5° . The symmetry of the distributions avoids under- or over-estimation in the wind inputs. Parameters used in the simulation are presented in Table 1.

3.2.1. Burnt area data acquisition

A drone survey was performed after the fire to map the affected perimeter, see Fig. 2(b). A DJI Mavic Dual Enterprise quadcopter (DJI, 2021), equipped with an FC2403 RGB digital camera, captured 867 nadiral images during drone missions over the burnt area. Photos were taken at varying altitudes (80 m and 60 m) with specific ground sampling distances (3.8 cm and $3.3 \text{ cm pixel}^{-1}$, respectively) and flight speeds of 5.0 m s^{-1} . Frontal lateral overlaps were maintained at 80% and 70%. The acquired images underwent processing using Agisoft

Metashape v.1.5.5 to generate orthophotos and Digital Surface Models (DSMs).

Details about the drone missions are reported in Table 2.

3.2.2. Evaluation methods

Following an approach commonly used in literature (see e.g. Filippi et al., 2014; Price and Germino, 2020), the Soersen coefficient and Cohen kappa are computed as measures of the agreement between the real and predicted burnt areas. Let \mathcal{B} be the burnt area in the real wildfire (i.e., the ground truth), and \mathcal{B}^{p_i} be the predicted burnt surface. p_i' denotes the possible threshold beyond the burning probability that can be considered by decision-makers. The Sorensen coefficient is defined as:

$$S_i^{p_i'} = \frac{2|\mathcal{B} \cap \mathcal{B}^{p_i'}|}{|\mathcal{B}| + |\mathcal{B}^{p_i'}|}, \quad (13)$$

where $|\cdot|$ denotes the area of a surface. Cohen Kappa, instead, measures the agreement between forecasted and real areas after removing

Table 1

List of the parameters and their values employed in the simulations.

Symbol	Name (units)	Value	Source
C_d	Drag coefficient.	0.47	Egorova et al. (2020)
c_p	Specific heat ($\text{J kg}^{-1} \text{K}^{-1}$).	2017	Tihay et al. (2009)
C_v	Wind parameter.	0.191	Alexandridis et al. (2011)
d	Unit depth of combustion zone (m).	1	Egorova et al. (2020)
g	Gravitational acceleration. (m s^{-2})	9.81	–
I_f	Fireline intensity (MW m^{-1}).	20	Alexander (1982)
L	Cell size (m)	20	Trucchia et al. (2020)
N_{FT}^2	Brunt-Väisälä frequency at the current height (μs^{-2}).	250	Sofiev et al. (2012)
N_0^2	Brunt-Väisälä frequency in the free troposphere (μs^{-2}).	278	Sofiev et al. (2012)
p	Percentile from z-tables; $z_p = 0.45$.	67	Egorova et al. (2020)
P_{f0}	Probability constant.	0.6	Alexandridis et al. (2011)
P_{cd}	Fuel type and density factor.	0.4	Alexandridis et al. (2011)
r	Mean firebrand radius (m).	0.015	Trucchia et al. (2019)
T_A	Ambient temperature (K).	308	IFS model (ECMWF) (Rodwell et al., 2021)
α	Measure of stability.	0.24	Sofiev et al. (2012)
β	Contribution of the fire intensity (m).	170	Sofiev et al. (2012)
β_2	Correction factor.	0.7	Egorova et al. (2020)
δ_{FT}	Dependence on stability of the free troposphere.	0.6	Sofiev et al. (2012)
η	Power-law dependence.	0.35	Sofiev et al. (2012)
ρ	Ambient air mass density (kg m^{-3}).	1.1	Egorova et al. (2020)
ρ_f	Density of spotting fuel (kg m^{-3}).	927	Tihay et al. (2009)

Table 2

Data from the UAV surveys.

Sub-area	Num. of images	Ground sampling distance (cm/pixel)	Flight altitude (m)	Time (start-end)
West	186	3.8	80	13:39–13:56
East	681	3.3	60	12:16–13:06
Total	867			

random agreements due to chance. It is defined as:

$$K^{p_i'} = \frac{P_a^{p_i'} - P_e^{p_i'}}{1 - P_e^{p_i'}}, \quad (14)$$

where

$$P_a^{p_i'} = \frac{|B \cap B^{p_i'}|}{|\mathcal{E}|} + \frac{|\mathcal{E} \setminus (B \cup B^{p_i'})|}{|\mathcal{E}|}, \quad (15)$$

$$P_e^{p_i'} = \frac{|B| |B^{p_i'}|}{|\mathcal{E}|^2} + \frac{|\mathcal{E} \setminus B| |\mathcal{E} \setminus B^{p_i'}|}{|\mathcal{E}|^2}, \quad (16)$$

and $\mathcal{E} \setminus *$ denotes the computational domain area, i.e., the cellular space \mathcal{E} , minus the surface $*$. Both scores range from 0 to 1. Values near 0 stand for low agreement while values close to 1 represent good agreement.

Finally, the simulation results are studied also in the framework of probabilistic analysis (Filippi et al., 2014; Allaire et al., 2021). In particular, routines for reliability and distribution of the probabilities are implemented (Allaire et al., 2020). A forecast is reliable, i.e., is well calibrated, if $\forall p \in [0, 1], f(p) = p$, where $f(p)$ is the distribution of the conditional probability $o|p$, where o stands for a real observation.

4. Analysis of the results

4.1. Synthetic test case results

Results under weak and strong wind conditions are provided. Figs. 4–6 portray the results of PROPAGATOR runs with the Alexandridis et al., Perryman et al. and RandomFront formulations, respectively. Synthetic tests are performed up to 9×10^3 s (150 min) of simulated time. The computational domain shown in Figs. 4, 5, and 6 remains consistent. The four sub-figures portrayed in Figs. 4, 5, and 6 correspond to the same time steps: 15, 30, 90, and 150 min, facilitating a more effective comparison of wildfire evolution under different spotting modules. For synthesis purposes, the plots depicting long-range effects, with varying extent of the computational domain, are shown in the *Supplementary Material*.

The outcome of this preliminary analysis shows the idealised spread patterns produced by the different spotting algorithms, where other sources of uncertainty are removed from the analysis. Under such idealised conditions, the spread capacity of the RandomFront and Alexandridis et al. parametrisations are higher. Additionally, the spotting effects in Alexandridis et al. do not scale with the fire size, whereas in Perryman et al. model and the RandomFront formulation long-distance spotting effects match with the size of the growth of the wildfire. When strong winds are considered, we observe that, at the end of the simulation, Alexandridis et al. and RandomFront parametrisations display a similar area characterised by high probability, while the patterns of low fire probability differ substantially. When Alexandridis et al. parametrisation is implemented, firebrands land near the fire-front if weak winds occur.

The final burnt area (ha) is shown in Table 3. We provide the burnt area at the 25%, 50%, 75% and 90% probability thresholds, as well as the averaged area. The averaged area is computed multiplying each burnt pixel by the burning probability assigned to that pixel. As expected, the influence of spotting on the burnt area increases with wind speed. We observe significant differences in the burnt area among models. These differences depend on the wind speed, but also on the probability thresholds. In Section 4.2, the three parameterisations are tested against a real-world scenario, with heterogeneous wind speed fuel cover and topography.

4.2. Real-wildfire simulations

We present in the following the results from the real-world case study. Figs. 7(a)–7(c) show the burning probabilities obtained by the fire-spotting models. Fig. 7(d) shows burning probabilities predicted without spotting, but retaining the same run settings. The simulations with the Alexandridis et al. model in Fig. 7(a) are implemented with the value of r_n , see Eq. (3), equal to 190 m, and standard deviation equal to 25 m. This was motivated by the width of the water body that is approximately equal to 190 m. Fig. 7(b) shows the results with the Perryman et al. model, and Fig. 7(b) portrays the burning probability map predicted by the RandomFront model.

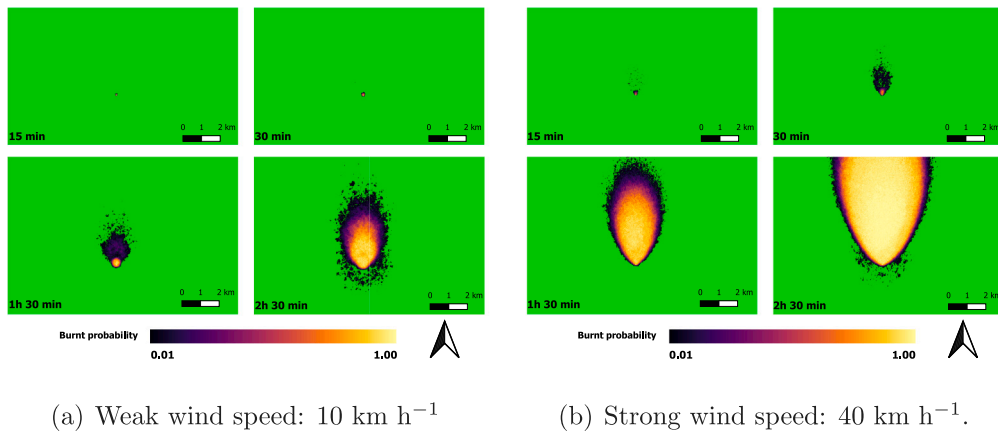


Fig. 4. Alexandridis et al. spotting model. Plot (a) shows the results under weak wind field, and Plot (b) under strong wind field. The wind direction originates from the South and remains unaltered for the entire duration of the simulation.

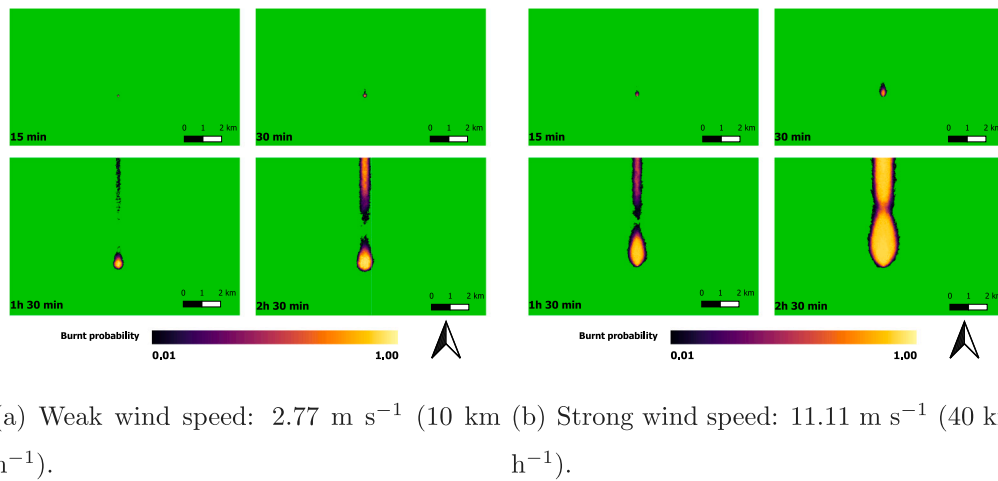


Fig. 5. Perryman et al. spotting model. Plot (a) shows the results under weak wind conditions, and Plot (b) under strong wind field. The wind direction originates from the South and remains unaltered for the entire duration of the simulation.

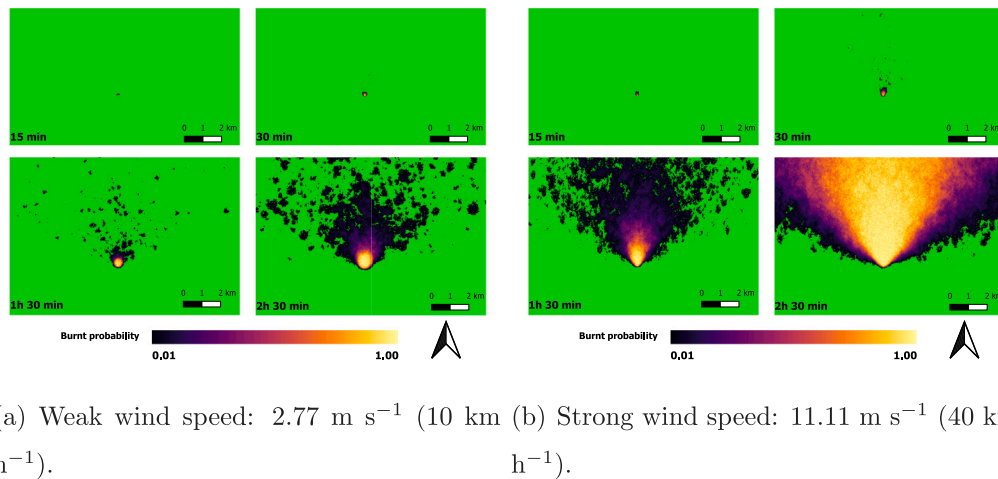


Fig. 6. RandomFront spotting model. Plot (a) shows the results under weak wind conditions, and Plot (b) under strong wind field. The wind direction originates from the South and remains unaltered for the entire duration of the simulation.

All the adopted formulations are able to reproduce the actual fire spread inside the East reference area. However, differences in the area affected by the spotting effects are accounted. Alexandridis et al. model predicts a uniform and low-probability spotting pattern, while the parametrisation proposed by Perryman et al. expresses an accurate

burnt area. However, probabilities in the pixels of the West reference area produced by spotting effects are still low. The pattern observed in Fig. 7(b) differs from the one observed in Figs. 5(a) and 5(b) due to the stochastic perturbations in the main wind direction and the more heterogeneous terrain and fuel setting. RandomFront parametrisation

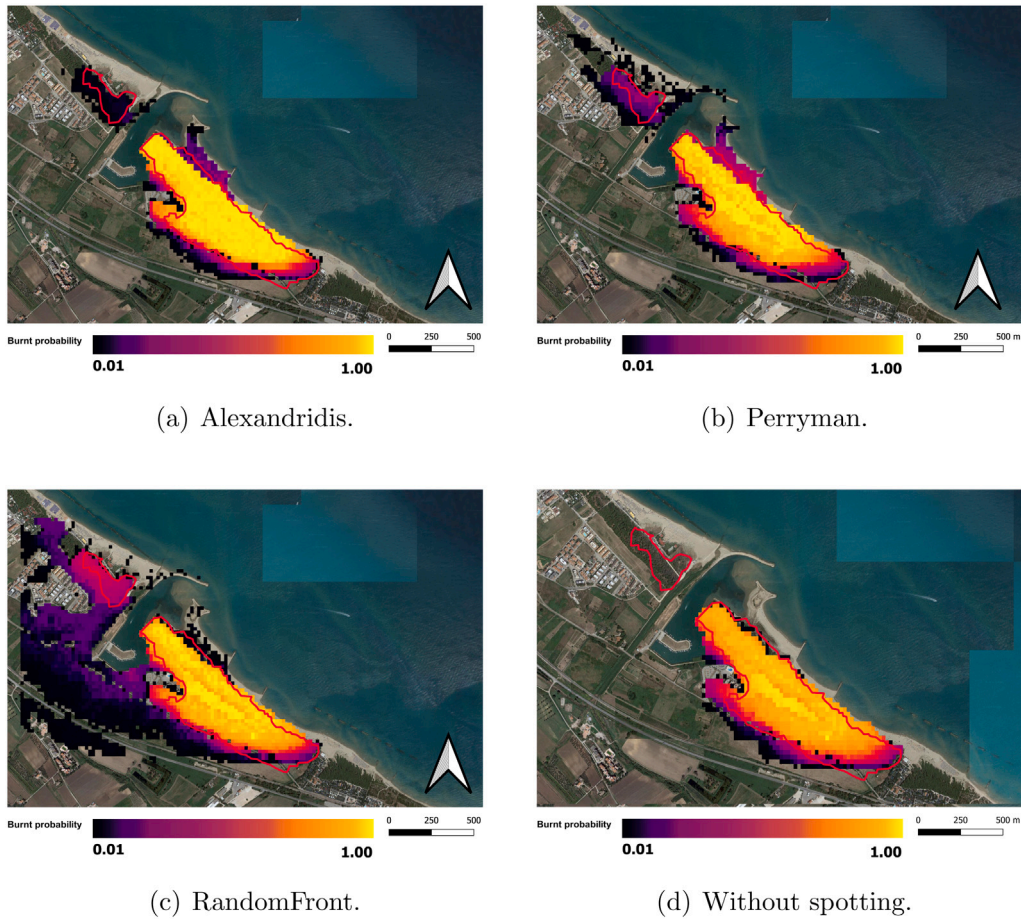


Fig. 7. Simulations with the Alexandridis et al., Perryman et al. and RandomFront firebrand landing models, and without spotting effects. All the plots are taken after 5 h of simulated time after the fire ignition.

Table 3

Area (ha) comparison for both weak and strong wind speed cases. Results corresponds with the simulations show in Figs. 4–6. For both cases, the burnt area held inside at the 25%, 50%, 75% and 90% probability iso-contours is provided, as well as the averaged area.

Model	Weak wind					Strong wind				
	25%	50%	75%	90%	Average	25%	50%	75%	90%	Average
Alexandridis	419.12	281.32	145.48	27.92	297.37	3099.24	2771.72	2333.96	1742.96	2637.81
Perryman	267.68	151.20	50.68	23.44	187.91	1236.08	1011.88	741.96	327.64	952.66
RandomFront	133.88	69.28	45.40	28.6	211.43	24345.72	8848.0	3027.56	1116.96	17861.62
Without spotting	58.64	47.96	33.64	13.44	44.49	208.52	173.92	1311.56	66.12	162.82

Table 4

Averaged probability inside the burnt areas. *West* reference area is the burnt area as consequence of the spotting effects and the *East* reference area is where the wildfire started. *Total* accounts for the whole burnt area observed.

Sub-model	East	West	Total
Alexandridis et al.	0.7938	0.0358	0.7090
Perryman et al.	0.7370	0.1330	0.6695
RandomFront	0.7303	0.2868	0.6801

generates a large number of low-probability burnt cells, while assigning a higher density of probability in the West reference area. We define the *averaged probability* as the sum of the probabilities associated to each cell inside a domain divided by the total number of cells of such domain. The resulting averaged probabilities from each model are reported in Table 4.

West domain in Table 4 shows that the RandomFront parametrisation forecast probabilities one order of magnitude higher than the Alexandridis et al. parametrisation, and twice than Perryman et al.

Fig. 8 illustrates the temporal evolution of the predicted burnt area, considering pixels as burnt when they reach thresholds of burning probability of at least 10%, 50%, and 75%, respectively.

Results show that the predictions for the main zone of the wildfire are not significantly affected by the use of different fire-spotting parametrisations. However, low probabilities are highly influenced.

Fig. 9 show the evolution of the Sorensen coefficient and Cohen Kappa defined in Eqs. (13), (14). We consider different probabilistic thresholds, observing strong dependence between both scores and the probability threshold. Fig. 10(a) shows the reliability diagram for the three models. The three models seem to be well calibrated for high probabilities, but for probabilities lower than 0.15 only RandomFront shows a good calibration. Finally, Fig. 10(b) portrays the distribution of the probabilities, also known as sharpness diagram (Allaire et al., 2021). Probabilities generated by RandomFront are mostly between 0 and 0.10, whereas Alexandridis et al. and Perryman et al. forecast higher probabilities than RandomFront.

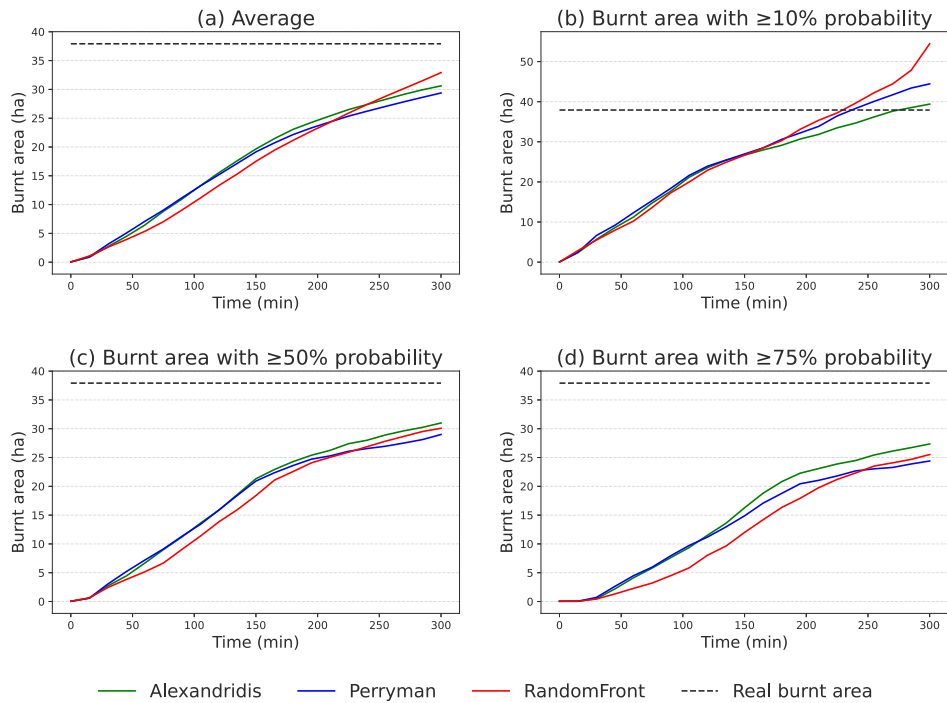


Fig. 8. Evolution of the burnt area over time. The black dashed line represents the 37.9 ha burnt in the real wildfire. Plot (a) shows the evolution of the averaged burnt area and plots (b), (c) and (d) show the evolution of the area with at least 10%, 50% and 75% of chances of burning.

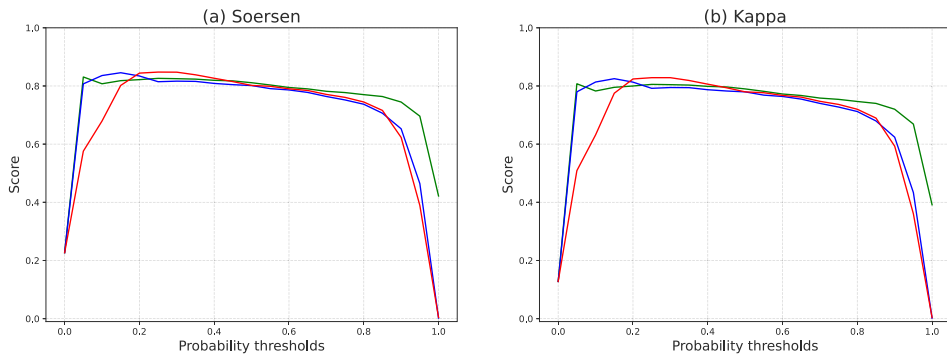


Fig. 9. Sorensen coefficient and Cohen kappa for each probability threshold.

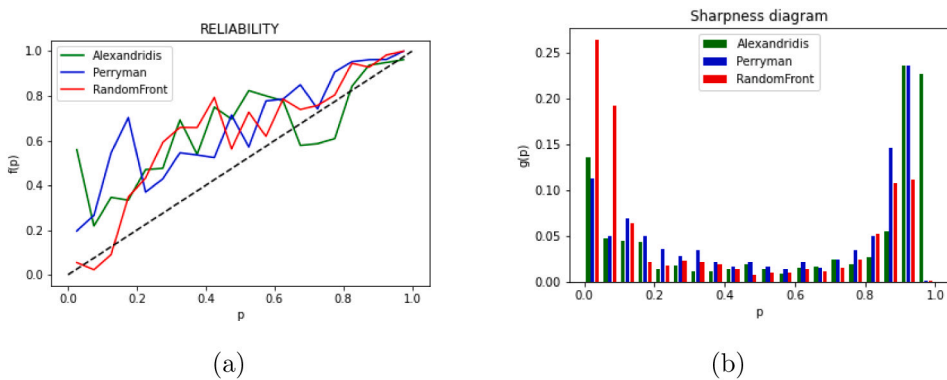


Fig. 10. Statistical analysis of the ensembles. Plot (a) shows the reliability diagram and Plot (b) the sharpness diagram.

5. Discussion

In the simulations conducted within the ideal framework, see Section 4.1, distinct spread patterns of burning probability emerged due

to the implementation of various spotting parametrisations. Among them, RandomFront exhibits the highest complexity, in the sense of spreading over longer ranges and in multiple directions. However, we also observe a notable risk of over-prediction in the wildfire evolution.

The model proposed by Alexandridis et al. shows limited capability in generating long-range spotting patterns. However, it exhibits a satisfactory spreading ability at short distances. On the other hand, simulations performed with the Perryman et al. model successfully generate long-range spotting effects. Nevertheless, its spread capacity shows a high correlation with the main wind direction.

Regarding the real-world case study, Fig. 7 highlights that results obtained with each model are substantially different. Among the analysed fire-spotting parametrisations, RandomFront emerges to be able to generate more diverse spread patterns. While the probabilities of fire occurrence are similar within the East reference area for all parametrisations, RandomFront resulted in higher predicted burning probabilities within the West reference area. However, we observe also a risk of over-prediction in the number of spot fires at short distances. Fig. 7(c) shows a significant number of cells with low burnt probabilities, which contrasts with the predictions from the two other parametrisations, see Figs. 7(a) and 7(b). The spread capacity of RandomFront appears to impact the agreement scores for low thresholds of probability, see Fig. 9.

Although fire spotting is challenging to be predicted, proper physical parametrisations can enhance the reliability of the burning probability maps provided by operational software codes for wildland fire simulation when fire-spotting phenomena occur.

The decision process based on the information obtained from each of the four PROPAGATOR settings of Fig. 7 (that is, one of the three different spotting parametrisations, and no spotting module at all) varies significantly. Particularly, overlooking the effects of fire-spotting in simulations appears to be negligent (see Fig. 7(d)). This aspect is particularly true for the real fire case study which evolves around a conifer fire in presence of strong winds, and with the field characterised by detached patches of fire prone vegetation. Moreover, in an operational setting, the presence of fire-spotting patterns excessively concentrated almost exclusively in a specific areas, as exhibited by Perryman et al. and Alexandridis et al. parametrisations, does not accurately reflect the full range of endangered exposed features that could be possibly affected by fire spotting.

Table 4 gives food for thought on the behaviour of PROPAGATOR adopting different spotting modules. As also evident from Fig. 7, RandomFront is the algorithm that associates the highest average probability of fire spread in the West reference area. Regarding the East reference area, it is evident that the other two algorithms put in place short-ranged spotting that raises the accumulated probability of fire spread in the eastern domain. RandomFront also exhibits short-range spotting in the primary ignition area, noticeable when comparing the probability distribution colours of RandomFront with those of the no-spotting PROPAGATOR runs.

In operational terms, a spotting algorithm that highlights more areas that could potentially receive burning embers, even though with a lower associated probability, can be useful for first responders since it adds more exposed assets to the list of priorities. For instance, Fig. 7(c) highlights some spotting probability on both sides of the highway 'SS 16 Adriatica'. Such wider probability coverage based on low probabilities was satisfactorily provided by RandomFront. Giving more importance to other possible spotting candidate areas, did not prevent Randomfront to correctly assign a higher probability density to the West reference area, where fire spotting occurred in the real wildfire event.

Operational software codes for wildfire simulations are mainly based on phenomenological and effective rules rather than on first principles and fundamental laws. However, as we show here, improvements in their probabilistic forecast are observed when the involved parametrisations are physically-based and the necessary physical constants and coefficients are fixed according to well-calibrated values. In this sense, a synergy with fully physics-based simulations (Tohidi and Kaye, 2017; Wadhvani et al., 2017, 2022b; Richards, 2010) is highly desired. In fact, notwithstanding their lack of operativeness as a consequence of the non-scalability of forest fires and the related computational costs, physics-based models can offer precise values of those constants and coefficients required by operational codes for reliable outputs.

6. Conclusions

Fire-spotting is one of the main sources of uncertainty and it is not properly taken into account in wildfire simulations. In this paper, it has been further demonstrated how spotting may cause significant discrepancies between simulated wildfires and observed wildfires. Nevertheless, the challenge of accurately integrating spotting modules into existing simulators is a significant task that cannot be ignored, regardless of the complexity of the process.

In this work the first implementation of fire-spotting modules in PROPAGATOR, an operational wildfire simulator based on CA, has been described. Event-based reconstruction of ember production and transport, as well as of secondary fire ignitions, represented a natural evolution of the grid based probabilistic algorithm that constitutes the core of PROPAGATOR, instead of requiring major re-writings of the code. Three distinct parametrisations of fire spotting have been tested, and one of them, namely RandomFront, has been adapted to a CA context for the first time. The results showed distinct spread patterns among the three studied parametrisations. A spread pattern based on low probabilities was observed with the RandomFront parametrisation. Moreover, RandomFront predicted a higher likelihood of burning in the area where the real wildfire occurred than the other two fire-spotting parametrisations. We conclude that physical parametrisations, such as the model developed by Pagnini and Mentrelli (2014), Trucchia et al. (2019) and Egorova et al. (2020, 2022), allow for long-range fluctuations of the burning probabilities and can increase the complexity of the fire spread patterns. The three proposed parametrisations are characterised by growing complexity and thus, by retaining the possibility to choose between them according to the available inputs, they can be a viable solution for PROPAGATOR. This is also the first time that PROPAGATOR is analysed not only for what regards the probability iso-contour (that is, analysing a sharp front advancing in time), since a comprehensive analysis of all the cells interested by a non null probability of fire burning at a given time is performed. This enabled a specific focus on areas characterised by a low probability of fire spread, where it is uncertain whether the fire will propagate or not, and therefore a certain potential for harm remains.

PROPAGATOR fire-spread simulator greatly benefited from the newly introduced modules, since it can now tackle a whole new class of scenarios where spotting play a key role. The SAFERS platform (SAFERS Consortium, 2020) already allows for adopting a fire-spotting module while requesting a new on-demand PROPAGATOR run.

Further steps will involve the improvement of the model's robustness by calibrating a suitable probabilistic density function for the firebrand generation process and the development of a physics-based probabilistic parametrisation of the spot-ignition mechanism.

CRedit authorship contribution statement

Marcos López-De-Castro: Conceptualization, Formal analysis, Investigation, Methodology, Software, Writing – original draft. **Andrea Trucchia:** Conceptualization, Funding acquisition, Investigation, Project administration, Resources, Supervision, Writing – review & editing. **Umberto Morra di Cella:** Conceptualization, Investigation. **Paolo Fiorucci:** Funding acquisition, Project administration, Resources, Supervision. **Antonio Cardillo:** Conceptualization, Resources. **Gianni Pagnini:** Conceptualization, Funding acquisition, Project administration, Supervision, Writing – review & editing.

Declaration of competing interest

The authors declare that they have no known competing financial interests or personal relationships that could have appeared to influence the work reported in this paper.

Data availability

Results of the simulations, the Python scripts of the performed analysis and supplementary material can be found at the following link: <https://gitlab.bcamath.org/malopez/fire-spotting.git>.

Acknowledgements

This research is supported by the Basque Government through the BERC 2022–2025 program, by the Spanish Ministry of Science and Innovation: BCAM Severo Ochoa accreditation CEX2021-001142-S/MICIN/AEI/10.13039/501100011033 and the project PID2019-107685RB-I00/MCIN/AEI/10.13039/501100011033, by the Spanish State Research Agency (AEI) through the project PDC2022-133115-I00 entitled “B₂ F₂: Be a Better digital Fire-Fighter” funded by MCIN/AEI/10.13039/501100011033 and by European Union ‘NextGenerationEU’/PRTR, and by the European Regional Development Fund (ERDF) and the Department of Education of the regional government, the Junta of Castilla y León, (Grant contract SA089P20). This work has been partially supported by the Interreg IPA CBC Italy-Albania-Montenegro programme through the project “The flood and Big fire fOEst, prediction, forecAst and emergencY management” (TO BE READY), and the Horizon 2020-funded project SAFERS “Structured Approaches for Forest Fire Emergencies in Resilient Societies” (H2020/Innovation Action), grant agreement No. 869353. The research activities described in this paper have been partially funded by the Italian “Piano Nazionale di Ripresa e Resilienza – PNRR”, Missione 4 Componente 2, Investimento 1.3 - D.D. 1243 2/8/2022, project RETURN “Multi risk science for resilient communities under a changing climate” - Partenariato Esteso PE00000005 - M.I.U.R. Ministry of Education and Merit.”

References

- Albini, F., 1979. Spot Fire Distance from Burning Trees -A Predictive Model. Research Paper INT-56, USDA Forest Service, Intermountain Forest and Range Experiment Station, Odgen, UT, <https://www.fs.usda.gov/treearch/pubs/32533>.
- Albini, F., 1983. Potential Spotting Distance from Wind-Driven Surface Fires. Research Paper INT-309, USDA Forest Service, Intermountain Forest and Range Experiment Station, Odgen, UT, <https://www.fs.usda.gov/treearch/pubs/32533>.
- Alexander, M., 1982. Calculating and interpreting forest fire intensities. *Can. J. Bot.* 60 (4), 349–357. <http://dx.doi.org/10.1139/b82-048>.
- Alexandridis, A., Russo, L., Vakalis, D., Bafas, G., Siettos, C., 2011. Wildland fire spread modelling using cellular automata: evolution in large-scale spatially heterogeneous environments under fire suppression tactics. *Int. J. Wildland Fire* 20 (5), 633–647. <http://dx.doi.org/10.1071/WF09119>.
- Alexandridis, A., Vakalis, D., Siettos, C., Bafas, G., 2008. A cellular automata model for forest fire spread prediction: The case of the wildfire that swept through spetses island in 1990. *Appl. Math. Comput.* 204 (1), 191–201. <http://dx.doi.org/10.1016/j.amc.2008.06.046>.
- Allaire, F., Filippi, J.-B., Mallet, V., 2020. Generation and evaluation of an ensemble of wildland fire simulations. *Int. J. Wildland Fire* 29 (2), 160–173. <http://dx.doi.org/10.1071/WF19073>.
- Allaire, F., Mallet, V., Filippi, J.-B., 2021. Novel method for a posteriori uncertainty quantification in wildland fire spread simulation. *Appl. Math. Model.* 90, 527–546. <http://dx.doi.org/10.1016/j.apm.2020.08.040>.
- Andrews, P., 1986. BEHAVE: Fire Behavior Prediction and Fuel Modeling System: Burn Subsystem, Part 1. General Technical Report INT-194, USDA Forest Service, Intermountain Research Station, Odgen, UT, <http://dx.doi.org/10.2737/INT-GTR-194>.
- Andrews, P., 2014. Current status and future needs of the BehavePlus fire modeling system. *Int. J. Wildland Fire* 23 (1), 21–33. <http://dx.doi.org/10.1071/WF12167>.
- Asensio, M.I., Ferragut, L., Álvarez, D., Laiz, P., Cascón, J.M., Prieto, D., Pagnini, G., 2021. PhyFire: An online GIS-integrated wildfire spread simulation tool based on a semiphysical model. In: Asensio, M.I., Oliver, A., Sarrate, J. (Eds.), *Applied Mathematics for Environmental Problems*. Springer International Publishing, Cham, pp. 1–20. http://dx.doi.org/10.1007/978-3-030-61795-0_1.
- Benali, A., Ervilha, A., Sá, A., Fernandes, P., Pinto, R., Trigo, R., Pereira, J., 2016. Deciphering the impact of uncertainty on the accuracy of large wildfire spread simulations. *Sci. Total Environ.* 569–570, 73–85. <http://dx.doi.org/10.1016/j.scitotenv.2016.06.112>.
- Bhutia, S., Ann Jenkins, M., Sun, R., 2010. Comparison of firebrand propagation prediction by a plume model and a coupled-fire/atmosphere large-eddy simulator. *J. Adv. Model Earth. Syst.* 2 (1), <http://dx.doi.org/10.3894/JAMES.2010.2.4>.
- Brown, A., Davis, K., 1973. *Forest Fire: Control and Use*. New York, McGraw-Hill.
- Calkin, D., Thompson, M., Finney, M., Hyde, K., 2011. A real-time risk assessment tool supporting wildland fire decisionmaking. *J. for.* 109 (5), 274–280. <https://www.fs.usda.gov/research/treearch/41565>.
- Clarke, K., Brass, J., Riggan, P., 1994. A cellular automaton model of wildfire propagation and extinction. *Photogramm. Eng. Remote Sens.* 60 (11), 1355–1367. <https://www.fs.usda.gov/research/treearch/41203>.
- DJI, 2021. Mavic 2 enterprise series user manual v 1.8. https://dl.djicdn.com/downloads/Mavic_2_Enterprise/20210413/Mavic_2_Enterprise_Series_User_Manual-EN.pdf. Accessed: February 27, 2024.
- Duarte, J., 1997. Bushfire automata and their phase transitions. *Int. J. Mod. Phys. C* 8 (2), 171–189. <http://dx.doi.org/10.1142/S0129183197000175>.
- Egorova, V., Trucchia, A., Pagnini, G., 2020. Fire-spotting generated fires. Part I: The role of atmospheric stability. *Appl. Math. Model.* 84, 590–609. <http://dx.doi.org/10.1016/j.apm.2019.02.010>.
- Egorova, V., Trucchia, A., Pagnini, G., 2022. Fire-spotting generated fires. Part II: The role of flame geometry and slope. *Appl. Math. Model.* 104, 1–20. <http://dx.doi.org/10.1016/j.apm.2021.11.010>.
- Encinas, L., White, S., del Rey, A., Sánchez, G., 2007. Modelling forest fire spread using hexagonal cellular automata. *Appl. Math. Model.* 31, 1213–1227. <http://dx.doi.org/10.1016/j.apm.2006.04.001>.
- Feranec, J., Soukup, T., Hazeu, G., Jaffrain, G., 2016. *European Landscape Dynamics: CORINE Land Cover Data*, first ed. CRC Press, <http://dx.doi.org/10.1201/9781315372860>.
- Fernandez-Pello, A.C., 2017. Wildland fire spot ignition by sparks and firebrands. *Fire Saf. J.* 91, 2–10. <http://dx.doi.org/10.1016/j.firesaf.2017.04.040>.
- Filippi, J., Mallet, V., Nader, B., 2014. Representation and evaluation of wildfire propagation simulations. *Int. J. Wildland Fire* 23 (1), 46–57. <http://dx.doi.org/10.1071/WF12202>.
- Finney, M., 1998. FARSITE, Fire Area Simulator—Model Development and Evaluation. Research Paper RMRS-RP-4, USDA Forest Service, Intermountain Research Station, Odgen, UT, <http://dx.doi.org/10.2737/RMRS-RP-4>.
- Freire, J., DaCamara, C., 2019. Using cellular automata to simulate wildfire propagation and to assist in fire management. *Nat. Hazards Earth Syst. Sci.* 19, 169–179. <http://dx.doi.org/10.5194/nhess-19-169-2019>.
- Hargrove, W., R.H., G., Turner, M., Romme, W., Despain, D., 2000. Simulating fire patterns in heterogeneous landscapes. *Ecol. Model.* 135 (2–3), 243–263. [http://dx.doi.org/10.1016/S0304-3800\(00\)00368-9](http://dx.doi.org/10.1016/S0304-3800(00)00368-9).
- Himoto, K., Iwami, T., 2021. Generalization framework for varying characteristics of the firebrand generation and transport from structural fire source. *Fire Saf. J.* 125, 103418. <http://dx.doi.org/10.1016/j.firesaf.2021.103418>.
- Himoto, K., Tanaka, T., 2005. Transport of disk-shaped firebrands in a turbulent boundary layer. *Fire Saf. Sci.* 8, 433–444. <http://dx.doi.org/10.3801/IAFSS.FSS.8-433>.
- Kaur, I., Mentrelli, A., Bosseur, F., Filippi, J.-B., Pagnini, G., 2016. Turbulence and fire-spotting effects into wild-land fire simulators. *Commun. Nonlinear Sci. Numer. Simul.* 39, 300–320. <http://dx.doi.org/10.1016/j.cnsns.2016.03.003>.
- Koo, E., Pagni, P., Weise, D., Woycheese, J., 2010. Firebrands and spotting ignition in large-scale fires. *Int. J. Wildland Fire* 19 (7), 818–843. <http://dx.doi.org/10.1071/WF07119>.
- Liu, N., Lei, J., Gao, W., Chen, H., Xie, X., 2021. Combustion dynamics of large-scale wildfires. *Proc. Combust. Inst.* 38 (1), 157–198. <http://dx.doi.org/10.1016/j.proci.2020.11.006>.
- Manzello, S., Maranghides, A., Mell, W., 2007. Firebrand generation from burning vegetation. *Int. J. Wildland Fire* 16 (4), 458–462. <http://dx.doi.org/10.1071/WF06079>.
- Manzello, S., Shields, J., Cleary, T., Maranghides, A., Mell, W., Yang, J., Hayashi, Y., Nii, D., Kurita, T., 2008. On the development and characterization of a firebrand generator. *Fire Saf. J.* 43, 258–268. <http://dx.doi.org/10.1016/j.firesaf.2007.10.001>.
- Manzello, S., Suzuki, S., Gollner, M., Fernandez-Pello, A., 2020. Role of firebrand combustion in large outdoor fire spread. *Prog. Energy Combust. Sci.* 76, 100801. <http://dx.doi.org/10.1016/j.pecs.2019.100801>.
- Pagnini, G., Mentrelli, A., 2014. Modelling wildland fire propagation by tracking random fronts. *Nat. Hazards Earth Syst. Sci.* 14 (8), 2249–2263. <http://dx.doi.org/10.5194/nhess-14-2249-2014>.
- Pérez, Y., Pastor, E., Águeda, A., Planas, E., 2011. Effect of wind and slope when scaling the forest fires rate of spread of laboratory experiments. *Fire Technol.* 47, 475–489. <http://dx.doi.org/10.1007/s10694-010-0168-7>.
- Peryman, H., Dugaw, C., Varner, J., Johnson, D., 2013. A cellular automata model to link surface fires to firebrand lift-off and dispersal. *Int. J. Wildland Fire* 22 (4), 428–439. <http://dx.doi.org/10.1071/WF11045>.
- Price, S.J., Germino, M., 2020. Modeling of fire spread in sagebrush steppe using FARSITE: an approach to improving input data and simulation accuracy. *Fire Ecol.* 18 (23), <http://dx.doi.org/10.1186/s42408-022-00147-2>.
- Richards, P., 2010. Steady aerodynamics of rod and plate type debris. In: *Proceedings of the 17th Australian Fluid Mechanics Conference*.

- Rodwell, M., Diamantakis, M., Düben, P., Janoušek, M., Lang, S., Polichtchouk, I., Prates, F., Roberts, C., Váňa, F., 2021. IFS upgrade provides more skillful ensemble forecasts. <https://www.ecmwf.int/en/newsletter/168/meteorology/ifs-upgrade-provides-more-skillful-ensemble-forecasts>. Last accessed: 6 November 2023. Newsletter Number 168 - Summer 2021, Published in July 2021.
- SAFERS Consortium, 2020. Structured approaches for forest fire emergencies in resilient societies (SAFERS). <http://dx.doi.org/10.3030/869353>, <https://cordis.europa.eu/project/id/869353>.
- Sardoy, N., Consalvi, J., Fernandez-Pello, A., Porterie, B., 2007. Modeling transport and combustion of firebrands from burning trees. *Combust. Flame* 150 (3), 151–169. <http://dx.doi.org/10.1016/j.combustflame.2007.04.008>.
- Sardoy, N., Consalvi, J., Kaiss, A., Fernandez-Pello, A., Porterie, B., 2008. Numerical study of ground-level distribution of firebrands generated by line fires. *Combust. Flame* 154 (3), 478–488. <http://dx.doi.org/10.1016/j.combustflame.2008.05.006>.
- Sofiev, M., Ermakova, T., Vankevich, R., 2012. Evaluation of the smoke-injection height from wild-land fires using remote-sensing data. *Atmos. Chem. Phys.* 12 (2), 1995–2006. <http://dx.doi.org/10.5194/acp-12-1995-2012>.
- Stephenson, C., Handmer, J., Betts, R., 2013. Estimating the economic, social and environmental impacts of wildfires in Australia. *Environ. Hazards* 12 (2), 93–111. <http://dx.doi.org/10.1080/17477891.2012.703490>.
- Storey, M., Price, O., Almeida, M., Ribeiro, C., Bradstock, R., Sharples, J., 2021. Experiments on the influence of spot fire and topography interaction on fire rate of spread. *PLoS ONE* 16 (1), e0245132. <http://dx.doi.org/10.1371/journal.pone.0245132>.
- Storey, M.A., Price, O.F., Sharples, J.J., Bradstock, R.A., 2020. Drivers of long-distance spotting during wildfires in south-eastern Australia. *Int. J. Wildland Fire* 29, 459–472. <http://dx.doi.org/10.1071/WF19124>.
- Sullivan, A., 2009a. Wildland surface fire spread modelling, 1990 - 2007. 1: Physical and quasi-physical models. *Int. J. Wildland Fire* 18 (4), 349–368. <http://dx.doi.org/10.1071/WF06143>.
- Sullivan, A., 2009b. Wildland surface fire spread modelling, 1990 - 2007. 2: Empirical and quasi-empirical models. *Int. J. Wildland Fire* 18 (4), 369–386. <http://dx.doi.org/10.1071/WF06142>.
- Sullivan, A., 2009c. Wildland surface fire spread modelling, 1990–2007. 3: Simulation and mathematical analogue models. *Int. J. Wildland Fire* 18 (4), 387–403. <http://dx.doi.org/10.1071/WF06144>.
- Sullivan, A., Cruz, M., 2015. Small-scale flame dynamics provide limited insight into wildfire behavior. *Proc. Natl. Acad. Sci. USA* 112 (31), E4164. <http://dx.doi.org/10.1073/pnas.1506877112>.
- Suzuki, S., Manzello, S., Lage, M., Laing, G., 2012. Firebrand generation data obtained from a full-scale structure burn. *Int. J. Wildland Fire* 21 (8), 961–968. <http://dx.doi.org/10.1071/WF11133>.
- Tarifa, C., de Noraio, P., Moreno, F., Villa, A., 1967. Transport and Combustion of Firebrands. Final Report of Grants FG-SP-114 and FG-SP-146. Technical Report Vol. II, INTA-Instituto Nacional de Técnica Aeroespacial, Madrid, <http://oa.upm.es/6521/>.
- Tarifa, C., del Notario, P., Moreno, F., 1965. On the flight paths and lifetimes of burning particles of wood. *Symp. (Int.) Combust.* 10 (1), 1021–1037. [http://dx.doi.org/10.1016/S0082-0784\(65\)80244-2](http://dx.doi.org/10.1016/S0082-0784(65)80244-2).
- Thomas, J., Mueller, E., Santamaria, S., Gallagher, M., El Housami, M., Filkov, A., Clark, K., Skowronski, N., Hadden, R., Mell, W., Simeoni, A., 2017. Investigation of firebrand generation from an experimental fire: Development of a reliable data collection methodology. *Fire Saf. J.* 91, 864–871. <http://dx.doi.org/10.1016/j.firesaf.2017.04.002>.
- Tihay, V., Simeoni, A., Santoni, P.-A., Rossi, L., Garo, J.-P., Vantelon, J.-P., 2009. Experimental study of laminar flames obtained by the homogenization of three forest fuels. *Int. J. Therm. Sci.* 48, 488–501. <http://dx.doi.org/10.1016/j.ijthermalsci.2008.03.018>.
- Tohidi, A., Kaye, N.B., 2017. Stochastic modeling of firebrand shower scenarios. *Fire Saf. J.* 91, 91–102. <http://dx.doi.org/10.1016/j.firesaf.2017.04.039>, *Fire Safety Science: Proceedings of the 12th International Symposium*.
- Tolhurst, K., Shields, B., Chong, D., 2008. Phoenix : development and application of a bushfire risk management tool. *Aust. J. Emerg. Manag.* 23, 47–54, <https://search.informit.com/doi/10.3316/agispt.20091124>.
- Trucchia, A., D'Andrea, M., Baghino, F., Fiorucci, P., Ferraris, L., Negro, D., Gollini, A., Severino, M., 2020. PROPAGATOR: An operational cellular-automata based wildfire simulator. *Fire* 3 (26), <http://dx.doi.org/10.3390/fire3030026>.
- Trucchia, A., Egorova, V., Butenko, A., Kaur, I., Pagnini, G., 2019. RandomFront 2.3: a physical parameterisation of fire spotting for operational fire spread models – implementation in WRF-SFIRE and response analysis with LSFIRE+. *Geosci. Model Dev.* 12 (69–87), 69–87. <http://dx.doi.org/10.5194/gmd-12-69-2019>.
- Trunfio, G., 2004. Predicting wildfire spreading through a hexagonal cellular automata model. In: Sloom, P., Chopard, B., Hoekstra, A. (Eds.), *Cellular Automata. ACR1 2004. Lecture Notes in Computer Science. Springer Berlin Heidelberg, Berlin, Heidelberg*, pp. 385–394. http://dx.doi.org/10.1007/978-3-540-30479-1_40.
- Tymstra, C., Bryce, R., Wotton, B., Taylor, S., Armitage, O., 2010. Development and Structure of Prometheus: The Canadian Wildland Fire Growth Simulation Model. Information Report NOR-X-417, Natural Resources Canada, Canadian Forest Service, Northern Forestry Centre, Edmonton, Alberta, <http://cfs.nrcan.gc.ca/publications?id=31775>.
- Wadhvani, R., Sullivan, C., Wickramasinghe, A., Matthew, K., Khan, N., Moinuddin, K., 2022a. A review of firebrand studies on generation and transport. *Fire Saf. J.* 134, 103674. <http://dx.doi.org/10.1016/j.firesaf.2022.103674>.
- Wadhvani, R., Sutherland, D., Ooi, A., Moinuddin, K., 2022b. Firebrand transport from a novel firebrand generator: numerical simulation of laboratory experiments. *Int. J. Wildland Fire* 31, 634–648. <http://dx.doi.org/10.1071/WF21088>.
- Wadhvani, R., Sutherland, D., Ooi, A., Moinuddin, K., Thorpe, G., 2017. Verification of a Lagrangian particle model for short-range firebrand transport. *Fire Saf. J.* 91, 776–783. <http://dx.doi.org/10.1016/j.firesaf.2017.03.019>, *Fire Safety Science: Proceedings of the 12th International Symposium*.
- Wang, H.-H., 2011. Analysis on downwind distribution of firebrands sourced from a wildland fire. *Fire Technol.* 47, 321–340. <http://dx.doi.org/10.1007/s10694-009-0134-4>.
- Werth, P., Potter, B., Clements, C., Finney, M., Goodrick, S., Alexander, M., Cruz, M., Forthofer, J., McAllister, S., 2011. Synthesis of Knowledge of Extreme Fire Behavior: Volume I for Fire Managers. Research Paper PNW-GTR-854, USDA Forest Service, Pacific Northwest Research Station, Portland, OR, <http://dx.doi.org/10.2737/PNW-GTR-854>.